JOURNAL OF CATALYSIS 55, 10–28 (1978)

Characterization of Cu/Al_2O_3 Catalysts

ROBERT MARK FRIEDMAN AND JOHN J. FREEMAN

Corporate Research Laboratories, Monsanto Company, St. Louis, Missouri 63166

AND

FARREL W. LYTLE

Boeing Company, Seattle, Washington 98124

Received February 27, 1978

The interaction of cupric ions with γ-alumina supports was studied by physical characterization of a wide range of catalyst preparations. The results from the different techniques, extended X-ray absorption fine structure (EXAFS), X-ray absorption edge shifts, X-ray diffraction, ESR, ESCA, and optical spectroscopy, were combined with prior work to develop a coherent description of the phases present and cation site distribution in the virgin and aged catalysts. Apparent inconsistencies between earlier workers are rationalized in terms of the present model and the details of the experimental probe used. A number of transition γ-aluminas appear to have a similar threshold loading for the appearance of crystalline cupric oxide, $\sim$4 wt% Cu/100 m^2/g support surface area. In the dispersed phase, the cupric ions are predominantly, but not exclusively, in a tetragonally distorted octahedral environment; there are some tetrahedrally coordinated ions present. The relative proportion of tetrahedral to octahedral cupric ions increases with time at calcination temperatures above 600°C until the cation distribution of bulk copper aluminate is reached; i.e., 60% tetrahedral and 40% octahedral sites.

INTRODUCTION

The state of cupric ions dispersed on alumina supports has been intensively studied by a variety of physiochemical techniques (*1–11*). This interest arises from its general performance as an oxidation catalyst, e.g., for the synthesis of glyoxal from glycol (*12*), as a promoter for the redox behavior of supported transition metal oxide catalysts, e.g., the reduction of Ni/Al_2O_3 catalysts (*13*), and to an overwhelming extent by its presence as a principal component of many of the base metal formulations for automobile exhaust emissions control developed over the last two decades (*14*). Unfortunately, there are some inconsistencies between the various results (*10*). These are further compounded by the fact that each technique was applied to different samples, adding yet another unknown factor into the development of a cogent model for the relationship between structure and catalytic behavior. In this and accompanying papers (*10, 15–19*), we formulate a unified picture of the interaction of the cupric ions with γ-alumina supports and discuss the implications of structure for catalytic performance and chemisorption. The present contribution describes the diverse results from X-ray diffraction, diffuse reflectance optical spectroscopy, ESCA, ESR, X-ray absorption

0021-9517/78/0551-0010$02.00/0

edge shifts, and extended X-ray absorption fine structure (*20*) (EXAFS) which are combined to yield a description of the phases present and the cation site locations in the virgin and aged catalysts.

EXPERIMENTAL METHODS

A series of catalysts was prepared by minimum solution impregnation of preformed γ-alumina supports by aqueous copper nitrate solutions. The preparations were oven-dried at 110°C overnight and then calcined at selected temperatures in a static air muffle furnace.

Two alumina supports were used in this study: Kaiser KA201 and Harshaw AL0104. The KA201 is a nodulized spherical material. In its "as received" form, it has not been conditioned at high temperature and is susceptible to thermal degradation. For several catalyst preparations, this support was calcined at 600°C for 6 hr prior to impregnation; otherwise, supports were merely oven-dried at 110°C. The Kaiser material was culled by hand of split spheres and sieved to 5×8 mesh. The Harshaw AL0104 is a thermally stabilized $\frac{1}{8}$-in. pellet. It showed no changes in surface area or textural properties upon being calcined at 600°C for several hours. Support properties are shown in Table 1. Table 2 summarizes the catalysts and some of their features. The precalcined Kaiser alumina is designated KA201(c).

Surface areas were determined by the multipoint BET method using an automated Micromeritics Digisorb 2500 instrument with N_2 as adsorbate (assumed cross section 16.2 Å^2).

Chemical analyses were performed by atomic absorption spectroscopy on samples totally dissolved by concentrated sulfuric acid digestion.

X-Ray diffraction powder patterns were obtained with Ni-filtered Cu $K\alpha$ radiation using a General Electric XRD-5 diffractometer. The output from the NaI crystal scintillation detector was integrated by a ratemeter and stored graphically with a stripchart recorder. The collection geometry assumed a flat plate, "infinite" thickness sample.

ESR spectra were obtained at X-band frequencies with a modified Varian V-4502 spectrometer equipped with a Fieldial II sweep unit, a 9 in. magnet, and with a TE102 rectangular or TE011 cylindrical cavity. Variable modulation frequencies were generated with a PAR-8 lock-in amplifier and amplified with a Krohn-Hite DCA-50 power amplifier.

ESCA spectra were measured using a Varian IEE-15 photoelectron spectrometer with base pressures $<10^{-6}$ Torr in the analyzer chamber. The samples were finely ground and mounted on the cylindrical aluminum holder using Scotch brand double-sided tape.

Diffuse reflectance spectra were obtained with a Cary 14 spectrophotometer fitted

TABLE 1

Support Properties

Material and treatment	Surface area (m^2/g)	% Na	Particle density (g/cm^3)	True density (g/cm^3)	Pore volume (cm^3/g)		
					Total	Micro[a]	Macro[a]
Kaiser KA201							
As received	306	0.27	1.2_0	3.1_0	0.51_0	0.40_9	0.10_1
600°C, 6 hr	165	0.27	1.2_2	3.3_7	0.52_5	0.40_2	0.12_3
Harshaw AL0104	75	0.19	1.5_2	3.4_3	0.36_7	0.25_1	0.11_6

[a] A pore diameter of 700 Å has been chosen as the division between micro- and macropores.

TABLE 2

Catalyst Preparations

Sample No.	Cu (wt%)	Support material	Calcination		Surface area (m^2/g)
			Temp. (°C)	Time (hr)	
1	1.8 ± 0.1	KA201(c)[a]	500	12	164 ± 3
2	6.1	KA201(c)	500	12	151
3	6.0	AL0104	500	12	80
4	3.7	KA201(c)	500	12	160
5	4.0	AL0104	500	12	83
6	3.6	KA201(c)	No. 4 + 600[b]	12	nd[c]
7	nd	AL0104	No. 5 + 600	12	nd
8	6.1	KA201(c)	No. 2 + 600	12	nd
9	6.0	AL0104	No. 3 + 600	12	nd
10	3.6	KA201	500	12	221
11	3.3	AL0104	500	12	86
12	3.3	AL0104	No. 11 + 900	12	55
13	4.9	KA201[d]	500	6	200
14	6.0	AL0104	No. 3 + 900	12	53
15	9.2	KA201	500	12	195
16	8.9	AL0104	500	12	79
17	9.2	KA201	No. 15 + 900	12	72
18	8.9	AL0104	No. 16 + 900	12	54
19	8.9	AL0104	500	12	73
20	16	AL0104	No. 19 + addtnl impregn		
			500	12	74
21	nd	AL0104	No. 19 + 900	12	nd
22	nd	AL0104	No. 20 + 900	12	nd

[a] KA201(c) is the Kaiser support calcined at 600°C for 6 hr prior to the impregnation step.
[b] No. n + = nth sample was subjected to the additional specified treatment.
[c] nd = not determined.
[d] This catalyst was prepared several years earlier on the "as received" Kaiser KA201 support.

with a Cary 1411 diffuse reflectance accessory. The accessory was equipped with a MgO-coated integrating sphere. To minimize the effect of particle size and specular reflection, samples were mixed in a steel ball mill with an equal weight of LiF (*21*). The finely ground mix was lightly compacted into a 3 mm deep well of an aluminum plate. The powdered sample surface was smoothed using a glass slide and the flat surface was mounted directly against the open port of the integrating sphere. Spectra were recorded in terms of the logarithm of the ratio of the LiF reflectivity to the sample reflectivity, $[\log_{10}(R_0/R)]$. A baseline of LiF versus LiF was also recorded for reference purposes.

X-Ray absorption data (edge and EXAFS) were collected with a modified Siemens diffractometer equipped with a conventional sealed Ag X-ray tube operating at 15 kV and 30 mA rectified, 0.1 mm incident and exit slits, a LiF (200) monochromator crystal, and a Xe-filled proportional counter. Scans were begun at $2\theta = 34.0°$ and proceeded with 0.01° steps in 2θ. The samples were maintained at 77 K. Spectra were obtained in fixed count-variable time mode with 10^5 counts per point per pass. Final data were the summation of 10 passes per sample. The

normal sample preparation procedure consisted of grinding the pellet, further pulverizing it in a Wig-L-Bug with acetone, mixing the slurry with Duco cement, spreading the composite on Al foil, and then folding the air-dried film on Al foil to sufficient thickness to serve as the absorber. Considering the problem of coincidence counting losses, a good sample thickness is characterized by $I_0/I = 3$. Precise details of the apparatus and procedure have previously described (*20*a).

RESULTS

X-Ray Diffraction

Both AL0104 and KA201 are γ-transition aluminas which show a broad peak at $\sim$37.4° 2θ (Cu $K\alpha$ radiation) in their XRD powder patterns. The two most prominent peaks for CuO are located at 35.6 and 38.8° 2θ (Cu $K\alpha$ radiation). This region is therefore very convenient to examine the evolution of the bulk oxide buildup as a function of copper loading. There is difficulty, however, in determining incipient bulk aluminate formation because both the aluminate and the γ-alumina are spinel-type phases and their diffraction peaks closely coincide. Nevertheless, qualitative interpretation of the diffraction patterns agrees with the composite of earlier findings (*1–3, 5*):

1. Low metal loading on moderate surface area supports (<3 wt% on 80 m^2/g) or moderate to high loadings on high surface area supports (5–10 wt% on 150–300 m^2/g) calcined at temperatures $\sim$500 to 500°C for $\leq$12 hr show no copper-containing phase.

2. Low temperature calcination ($\leq$600°C) of high loadings (>4 wt%/100 m^2/g) may show copper oxide but not bulk copper aluminate.

3. XRD powder patterns of samples calcined at 900°C show both bulk aluminate and α-Al_2O_3. At the highest loading studied (16 wt% Cu in sample No. 22), only $CuAl_2O_4$ was detected.

The threshold level for the appearance of CuO seems to be abrupt and generally related to the surface area of the support. None of the preparations using KA201 shows any significant CuO by XRD. The powder pattern of sample No. 2 (6.1% Cu/KA201(c)/500°C) does, however, show the appearance of the oxide. The behavior of AL0104 is markedly different as illustrated in Fig. 1A. The height of the major CuO diffraction peak (normalized to the alumina diffraction) plotted as a function of metal loading shows remarkable linearity (Fig. 1B).

ESR

The intensity of the Cu^{2+} ESR signals for the different catalysts were standardized relative to a $CuSO_4 \cdot 5H_2O$ single crystal. The results reproduce the findings of Matsunaga (*22*) and others (*2, 3*)[1]; i.e., there is a significant decrease in the relative ESR signal intensity per cupric ion as the metal loading is increased. The results for catalysts prepared with different supports, A10104 or virgin or precalcined KA201, follow this same general trend. The only ESR signal observed is that previously interpreted as arising from a tetragonally distorted octahedrally coordinated $(C_{4v})Cu^{2+}$ ion (*2*).

ESCA

ESCA measurements made on some of the catalysts yielded initially surprising results (see Table 3). Previous work (*4*) had shown a clear identification of the predominant copper-containing phase present in the catalyst using the Cu $2p_{\frac{3}{2}}$ binding energy. Our measurements, even on sample Nos. 16 and 19 with moderately high Cu

[1] The labeling in Fig. 3 of Ref. (*2*) is incorrect, notation $a \rightarrow d$ should be reversed (P. A. Berger, Monsanto Co., private communication).

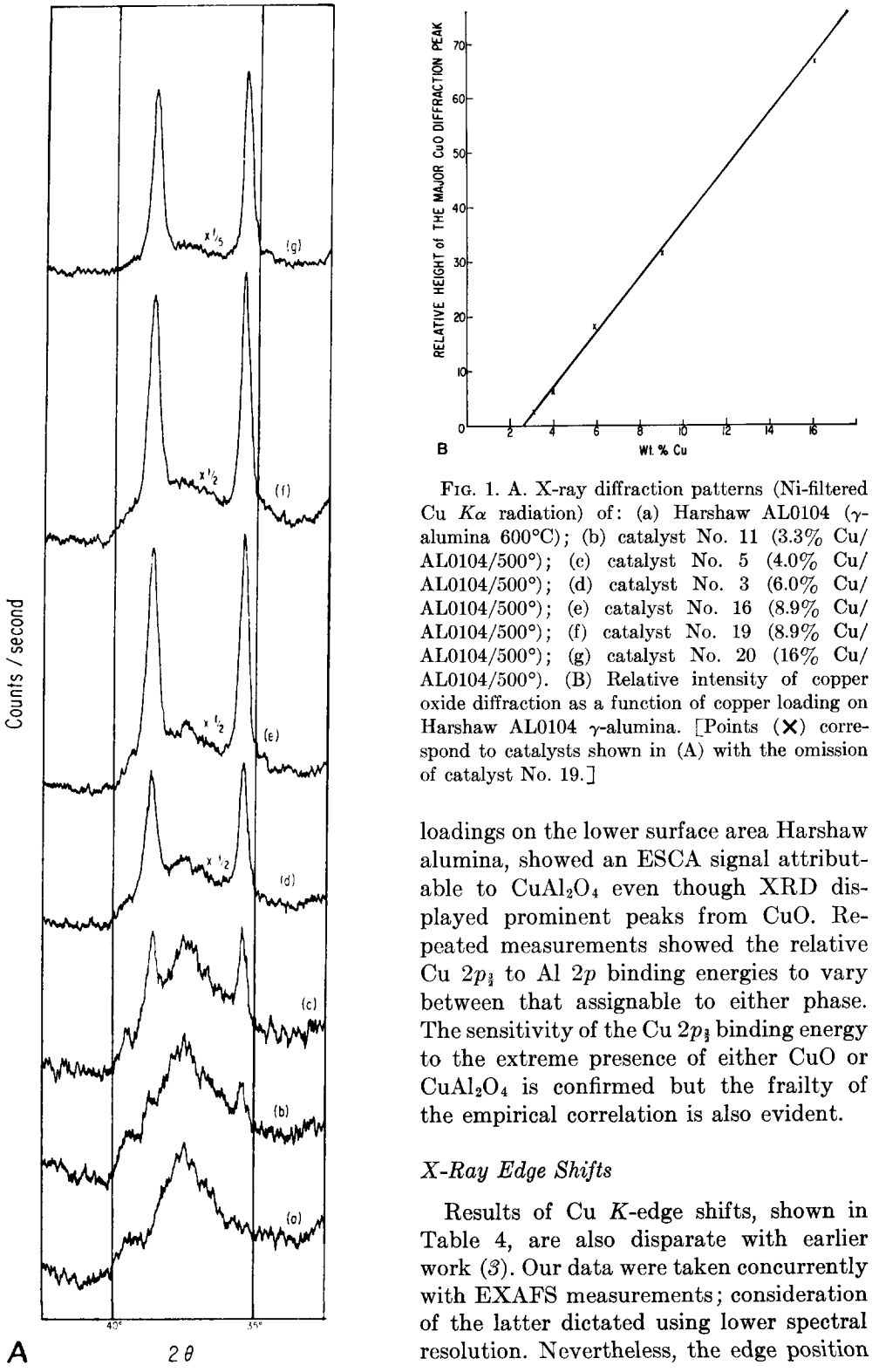

FIG. 1. A. X-ray diffraction patterns (Ni-filtered Cu $K\alpha$ radiation) of: (a) Harshaw AL0104 (γ-alumina 600°C); (b) catalyst No. 11 (3.3% Cu/AL0104/500°); (c) catalyst No. 5 (4.0% Cu/AL0104/500°); (d) catalyst No. 3 (6.0% Cu/AL0104/500°); (e) catalyst No. 16 (8.9% Cu/AL0104/500°); (f) catalyst No. 19 (8.9% Cu/AL0104/500°); (g) catalyst No. 20 (16% Cu/AL0104/500°). (B) Relative intensity of copper oxide diffraction as a function of copper loading on Harshaw AL0104 γ-alumina. [Points (×) correspond to catalysts shown in (A) with the omission of catalyst No. 19.]

loadings on the lower surface area Harshaw alumina, showed an ESCA signal attributable to $CuAl_2O_4$ even though XRD displayed prominent peaks from CuO. Repeated measurements showed the relative Cu $2p_{\frac{3}{2}}$ to Al $2p$ binding energies to vary between that assignable to either phase. The sensitivity of the Cu $2p_{\frac{3}{2}}$ binding energy to the extreme presence of either CuO or $CuAl_2O_4$ is confirmed but the frailty of the empirical correlation is also evident.

X-Ray Edge Shifts

Results of Cu K-edge shifts, shown in Table 4, are also disparate with earlier work (*3*). Our data were taken concurrently with EXAFS measurements; consideration of the latter dictated using lower spectral resolution. Nevertheless, the edge position

was easily determined as the first maximum in the derivative of the digitized spectra. Comparison of these positions with the $WL_{\beta 1}$, $WL_{\beta 2}$, and $CuK_{\beta 1}$ impurity X-rays establish the 2σ error of ± 0.5 eV as a measure of both the precision and accuracy. Qualitative comparison of the data shows sample Nos. 2, 16, and 18 to be nominally aluminate, whereas sample No. 20 appears to be a mixture of the oxide and aluminate phases. The earlier work more clearly differentiated between phases. This is a consequence of the alternate method of locating the edge in the graphically displayed data. The prior work used the absorption onset determined from the intersection of the tangents to the curve above and below that point (*3*).

TABLE 3

ESCA Cu $2p_{\frac{1}{2}}$ Binding Energies

Sample No.	Cu $2p_{3/2}$ binding energy[a] (eV)	Assignment
CuO[b]	933.6	
$CuAl_2O_4$	934.6	
1 (1.8% Cu/KA201(c)/500°)	934.2	$CuAl_2O_4$
2 (6.1% Cu/KA201(c)/500°)	934.5	$CuAl_2O_4$
3 (6.0% Cu/AL0104/500°)	934.4	$CuAl_2O_4$
16 (8.9% Cu/A10104/500°)	934.8	$CuAl_2O_4$
19 (8.9% Cu/A10104/500°)	934.4$_5$	$CuAl_2O_4$
	933.8$_5$	CuO
	934.0$_5$	CuO/$CuAl_2O_4$ mixture
20 (16% Cu/A10104/900°)	933.7	CuO

[a] Binding energies quoted have been corrected relative to Al $2p$ = 74.0 eV.

[b] The CuO sample is a physical mixture with γ-alumina.

Diffuse Reflectance Optical Spectroscopy

Before presenting the results, a brief explanation must be given regarding the form of the data which were acquired by the diffuse reflectance technique (*24*). The Cary 14 spectrophotometer recorder displays log (R_0/R) where R_0 and R are the reflectance from the reference and sample, respectively. This data presentation does not relate the reflectance to an analog of the Beer–Lambert law familiar from transmittance spectroscopy. A phenomenological theory has been developed which transforms the data to this desired relationship. It is known as the Schuster–Kubelka–Munk (SKM) equation which for sufficiently thick samples takes the form:

$$\frac{(1-R)^2}{2R} = \frac{\kappa}{\sigma},$$

TABLE 4

X-Ray K-Edge Shifts

Material	Relative edge position (eV)	Other work	
		Position (eV)	Ref.
Copper metal	0.0 ± 0.5	0.0	
Cu_2O	−0.7	−0.67	(*23*)
CuO	3.6	3.87	(*23*)
		3.86	(*3*)
$CuAl_2O_4$	5.9	7.94	(*3*)
Sample No. 2 (6.1% Cu/KA201(c)/500°)	5.8		
Sample No. 18 (8.9% Cu/AL0104/900°)	6.2		
Sample No. 16 (8.9% Cu/AL0104/500°)	6.1		
Sample No. 20 (16% Cu/AL0104/500°)	5.1		
3.35 wt% Cu/Kaiser XA331[a]		7.94	(*3*)
8.8 wt% Cu/Kaiser XA331		7.73	(*3*)
10.5 wt% Cu/Kaiser XA331		7.94	(*3*)
10.3 wt% Cu/AL0104		4.5	(*3*)

[a] Kaiser XA331 is a high surface area (N_2 BET 301 m^2/g) γ-alumina.

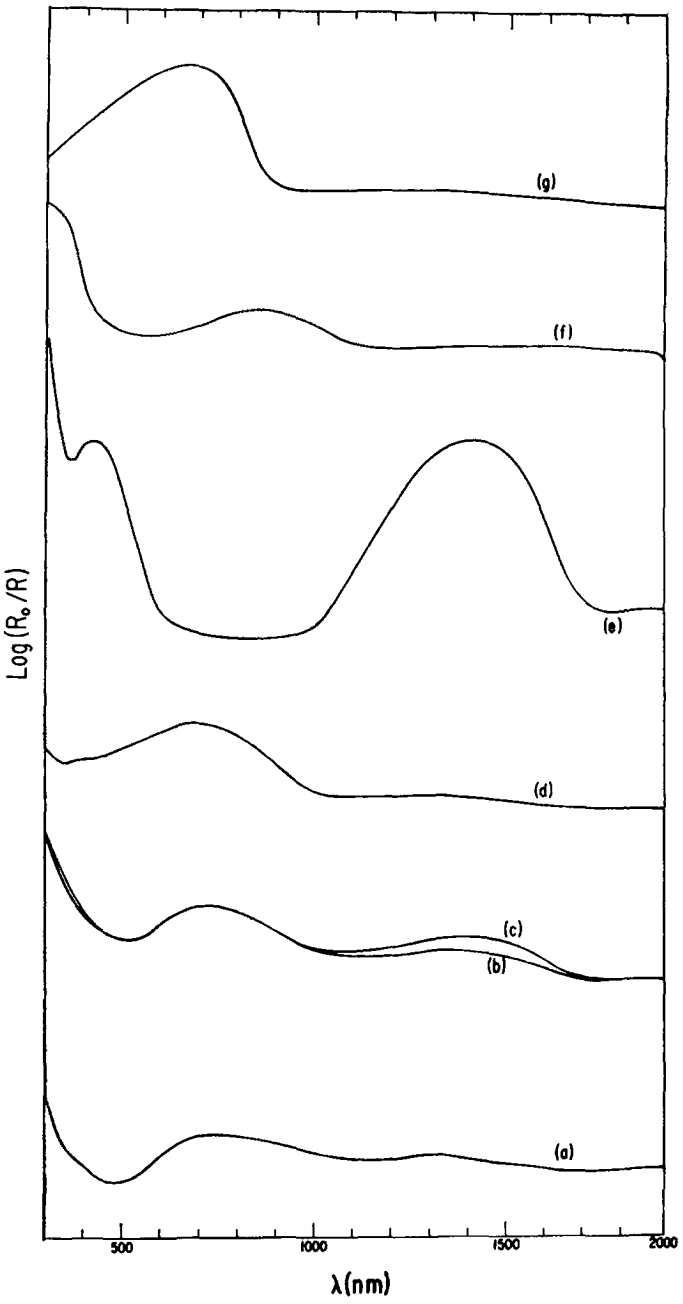

FIG. 2. Diffuse reflectance spectra of: (a) catalyst No. 1 (1.8% Cu/Ka201(c)/500°); (b) catalyst No. 4 (3.7% Cu/KA201(c)/500°); (c) catalyst No. 6 (3.6% Cu/Ka201(c)/600°); (d) catalyst No. 20 (16% Cu/AL0104/500°); (e) $CuAl_2O_4$; (f) Cu-doped in MgO; (g) CuO.

where R is the reflectance of a sample of infinite thickness, κ is the absorption coefficient, σ is the scattering coefficient per unit path length, and the expression $(1 - R)^2/2R$ is called the remission coefficient. Furthermore, plotting the logarithm

of the remission coefficient versus wavenumber allows comparison of different spectra by shifting the ordinate by $(-\log \sigma)$.

Representative optical spectra are shown in Fig. 2. The graphical spectra were digitized using a Grafacon 1010A curve digitizer and then processed to the form consistent with the SKM equation. Qualitative relationships are apparent from the experimental data, but further quantification relies on analysis of the transformed data. Three catalyst samples look similar, Fig. 2a–c, No. 2 (1.8% Cu/KA201(c)/500°), No. 4 (3.7% Cu/AL0104/500°), and No. 6 (3.6% Cu/AL0104/600°), respectively; but the catalyst with the highest metal loading, Fig. 2d, No. 20 (16% Cu/AL0104/500°) is significantly different.

For comparison, Cu^{2+} in an "octahedral" environment has a low wavelength band between 600 and 900 nm, exemplified by the Cu-doped in MgO spectra, Fig. 2f, whereas cupric ions in a "tetrahedral" environment have an absorption band between 1300 and 1600 nm, the predominant feature of the $CuAl_2O_4$ spectra (Fig. 2e). Copper oxide is a semiconductor with an onset of interband transitions at 900 nm and a peak in this distribution at 700 nm (Fig. 2g). The pure cubic coordination of Cu^{2+}, either T_d or O_h, should be unstable according to the Jahn–Teller theorem. The above generalities on band locations allow for small distortions; however, significant reduction in the symmetry leads to splitting of the absorption bands. Kassman (*9*) has calculated the effect of the octahedral (O_h) to square pyramidal (C_{4v}) distortion. He notes that in the lower symmetry there are two ligand field bands; one in the region ascribed to octahedral symmetry and a weaker component in the region ascribed to a tetrahedral field.

All catalysts showed spectra with bands in the higher and lower wavelength regions, consistent with both octahedrally and tetrahedrally coordinated cupric ions. This is discussed further below. Accepting this assignment of the bands, we can use the transmission data of Pappalardo (*25*) for an order of magnitude quantification of the results. The oscillator strength of Cu-doped in ZnO (T_d) is 20 times that of $CuSiF_6 \cdot 6H_2O$ (O_h), reflecting the effect of the center of symmetry in the octahedral environment. It is clear from the transformed data that on both supports there is a much higher concentration of octahedrally coordinated cupric ions than the less plentiful, but always present, tetrahedrally coordinated ions $[Cu(O_h)/Cu(T_d) \approx 10:1]$.

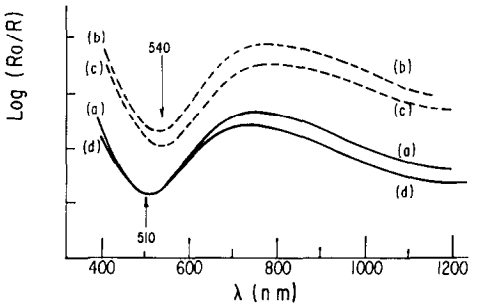

FIG. 3. Diffuse reflectance spectra of Cu/Al_2O_3 catalyst No. 10 (3.6% Cu/KA201/500°) (relative absorbance between samples is not significant): (a) 25 Torr NH_3 exposure at equilibrium; (b) sample a reevacuated by heating; (c) fresh sample; (d) 500 Torr NH_3 exposure at equilibrium.

The changes in the Cu^{2+} optical spectrum upon adsorption of ammonia are informative about the accessibility of the cupric ions. Figure 3 shows the diffuse reflectance spectra with and without adsorbed NH_3 on catalyst No. 10. There is a small but reproducible shift in the minimum on the low wavelength side of the octahedral band reflecting increased optical absorption in this higher energy region. The tetrahedral region is unchanged (not shown). The spectra are displayed without significance for the relative absorbance between the difference samples.

EXAFS

EXAFS are the small oscillations in the X-ray absorption coefficient as a function

of energy extending upwards from 50 eV above a characteristic absorption edge of an atom in the environment of other atoms. The origin of these features is the interference between the component of the ejected photoelectron elastically backscattered by neighboring atoms and the photoelectron wave propagating outward from the absorption center. These waves can either be in-phase, resulting in constructive interference with a concomitant increase in X-ray absorption, or out-of-phase, hence destructive with a decrease in absorption. The interference pattern, EXAFS, $\chi(k)$, has a frequency which depends on:

1. The distance between the absorbing atom and its surrounding coordination spheres.
2. A phase shift associated with the photoionization and scattering processes.

and an amplitude reflecting:

1. The number of scattering atoms.
2. The identity of the absorber and neighbor.
3. The dynamic and static disorder in the internuclear distances.

This periodic function can be Fourier transformed to yield a pseudo-charge distribution $\phi(r)$. Our application of EXAFS to the understanding of Cu/Al_2O_3 catalysts utilizes this approach to data analysis.

The oscillations were isolated; any overall slope was removed; then, they were normalized prior to Fourier transformation. The main stepfunction and monotonic variation were removed by subtracting a Victoreen fit to the data below the edge and a parabolic fit to the general slope above the edge followed by Fourier filtering. The programs and techniques used have been described (*20*) except for an improvement in the "window function."

The Fourier analysis of EXAFS is complicated by the finite range and termination of the data set which is manifested in nonphysical side lobes, called Gibbs oscillations, about the true peak. To minimize this effect, the data are smoothly and artificially brought to zero at the limits, k_{min} and k_{max}, by multiplication by a window function. This results in a final radial distribution function which is the convolution of the Fourier transform of the window function with the transform of the data (*25*). The effect of this smoothing is a loss of resolution. An effective compromise between these competing features is a Hanning function (*27*). It was applied in such a way that the central portion of the data was unchanged while the initial and final 10% of the range was multiplied by the function $\frac{1}{2}\{1 - \cos 2\pi[(k - k_{min})/(k_{max} - k_{min})]\}$. This makes the data follow a smooth, half-cosine bell curve down to $\chi(k) = 0$ at k_{min} and k_{max}. All data, for reference materials and catalysts, were treated in this manner. Furthermore, the current data have a fairly high noise level as well as residual noise from the coincidence loss correction. These noise spikes were best handled by introducing an artificial temperature term, $\exp(-0.005\,k^2)$. The effects are to slightly reduce the resolution and amplitude of the transform and to minimize the ripple effects which can run through the entire data.

There are some qualitative considerations to be noted in transforming data: (a) range of transform, (b) exponent of k used to multiply $\chi(k)$, and (c) general quality of data. The optimal values for k_{min} and k_{max} are not the same for all data, but the validity of comparisons requires that the transforms be taken over the same range with the same data reduction. Stern (*28*) has noted the desirability of using k^3 transforms; however, any k^n transform will contain the same frequency structure but will be k-weighted differently. The effect of increasing n is to weight the transform to the high k-region of the EXAFS which produces the best resolution and accuracy in a manner similar to the effect of high order diffraction lines; however, this is also the region of greatest error in the data

and multiplication by k^3 will increase the noise level of the transform. For the catalysts studied in this work, the EXAFS signal dampens out quickly and the best results were obtained with the k^1 transforms which were used throughout. Various transforms were performed within the range $2 \leqslant k \leqslant 20$ encompassing the normalized data. The most consistent set of results were obtained for $2 \leqslant k \leqslant 20$ and $2 \leqslant k \leqslant 11$; the final coordination numbers and distances represent an average of values from these regions. The range $4.1 \leqslant k \leqslant 11$ yielded transforms with better resolution of various peaks; therefore, they were used to fingerprint identification of various components. However, these data could not be used for accurate quantification since they omit part of the first EXAFS peak.

The analysis of the data proceeds by (a) fingerprints, (b) inferences from the expected site symmetry in γ-Al_2O_3, and (c) quantitative assignment of cupric ions to the spinel model coupled with results from other physical techniques. For the latter, the frequency and amplitude information enumerated above was parameterized using standards to yield coordination distances and numbers. CuO, Cu_2O, CuCl, and CuS served as standards for nonmetal atom near neighbors, whereas data from copper metal and Cu_2O served to parameterize metal atom neighbors. Using the linear phase approximation (*20*), phase shifts associated with the photoionization and scattering processes result in a transferable displacement of the origin of the radial scale. The transform yields a real part, an imaginary part, and the magnitude or modulus; only the latter is discussed in this work. The equation for the radial structure function is:

$$\phi(r) = \sum_{\text{coord shells } j} \frac{N_j t_j(2k)}{r_j^2 \sigma_j} \exp[-2r_j/\lambda] \exp[-(r - r_j)^2/2\sigma_j^2], \quad (1)$$

where

- N_j the coordination number of the jth coordination shell;
- $t_j(2k)$ the transform of the backscattering amplitude;
- λ the mean free path of the photoelectron in the solid;
- r_j the corrected coordination distance of the jth shell;
- σ_j the pseudo-Debye–Waller factor relating to the static and dynamic disorder in the distance r_j.

Minimizing thermal effects by obtaining all data at 77 K, the effective coordination number for an element in a catalyst was evaluated by grouping the unknown amplitude terms into a pseudo-constant and assuming transferability from standards to the catalysts (*29*a); i.e., from [Eq. (1)]:

$$(\text{Magn})_{r_{j,\text{std}}} = \frac{C_j N_{j,\text{std}}}{r^2_{j,\text{std}}}, \quad (2a)$$

$$C_j = \frac{(\text{Magn})_{r_{j,\text{std}}}(r^2_{j,\text{std}})}{N_{j,\text{std}}}, \quad (2b)$$

$$N_{j,\text{unknown}} = \frac{(\text{Magn})_{j,\text{unknown}}(r^2_{j,\text{unknown}})}{C_j}. \quad (2c)$$

This assumption was tested for consistency by comparing results for the three different transform ranges and between the different standard materials. Its success reflects: (a) the low temperature of measurement, hence minimizing the effects of dynamic disorder; (b) the relatively high error bounds quoted for the numbers deduced by this method which hides many of its inadequacies, including static disorder; and (c) the high correlated motion between the metal center and its first coordination sphere, its most applicable case.

Qualitative examination of the $4.1 \leqslant k \leqslant 11.0$ transforms (Fig. 4) reveals similar EXAFS spectra of CuO and $CuAl_2O_4$. This

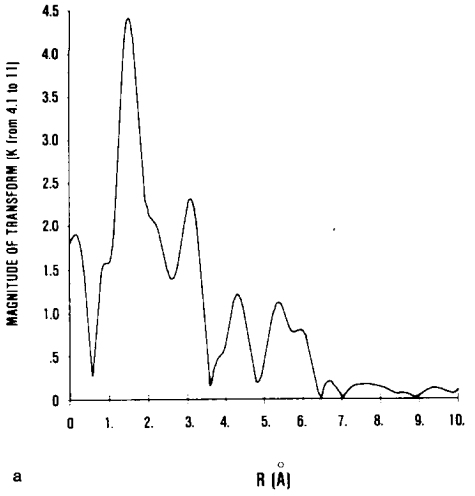
MAGNITUDE OF TRANSFORM (K from 4.1 to 11)
R (Å)

a

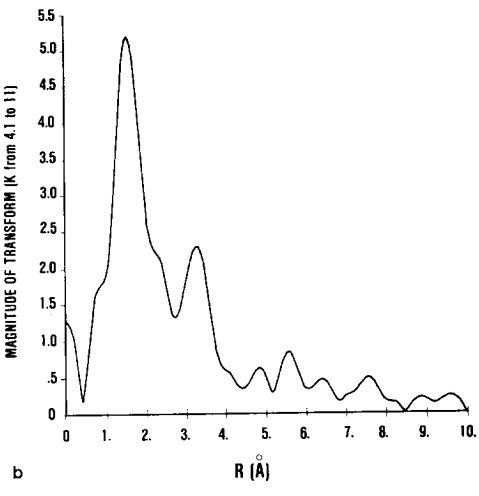
MAGNITUDE OF TRANSFORM (K from 4.1 to 11)
R (Å)

b

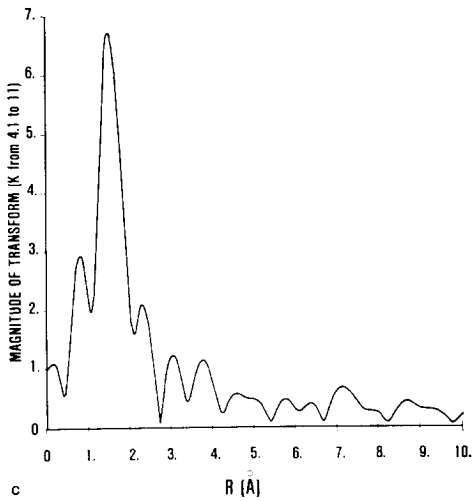
MAGNITUDE OF TRANSFORM (K from 4.1 to 11)
R (Å)

c

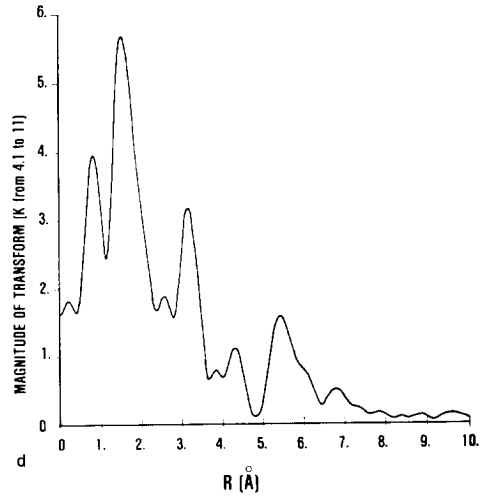
MAGNITUDE OF TRANSFORM (K from 4.1 to 11)
R (Å)

d

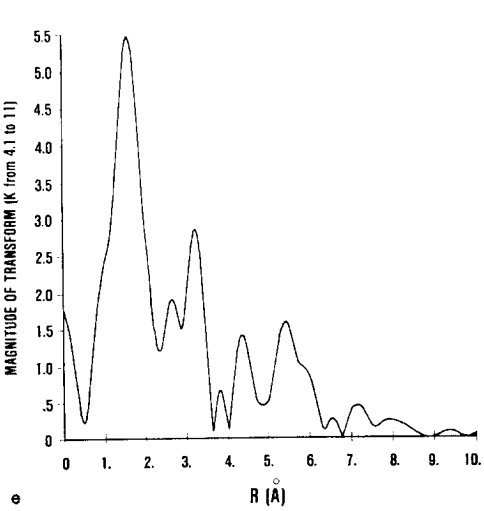
MAGNITUDE OF TRANSFORM (K from 4.1 to 11)
R (Å)

e

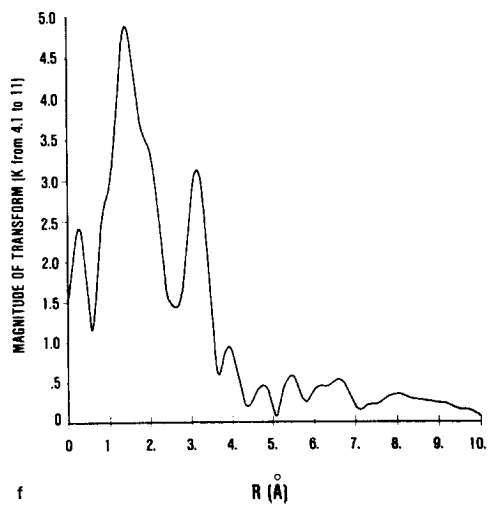
MAGNITUDE OF TRANSFORM (K from 4.1 to 11)
R (Å)

f

is not surprising since in both cases the cupric ions are in an oxygen lattice. There are sufficient differences, however, to identify two forms of Cu coordination in the catalyst samples. The catalyst Nos. 16 and 20 show considerable CuO and spinel aluminate. Note especially the peaks characteristic of CuO in the region 4 to 6 Å. When catalyst No. 16 was heated to 900°C, resulting in catalyst No. 18, the CuO phase disappears and the $CuAl_2O_4$ lines are very sharp. Catalyst No. 2, a lower copper loading on the high surface area support, is qualitatively different from the other materials; namely, there are no appreciable peaks attributable to long range ordering. This is also true for the transforms over a wider range in k (see Fig. 5).

γ-Al_2O_3 is a defect spinel, whereas bulk $CuAl_2O_4$ is a partially inverse cubic spinel (*15*). Using the spinel structure (space group $Fd3m$) and copper aluminate lattice parameters, we have calculated the coordination numbers and distances surrounding octahedral and tetrahedral metal ion sites. The most apparent difference between them is the presence of another metal ion site at 2.8 Å from the octahedral site. This peak is located at 2.5 Å in the transforms when the phase shift is included. The peak at 3.0 Å in the transform is expected to be considerably more intense for tetrahedrally coordinated Cu^{2+}. In the latter environment, this peak reflects both oxygen and other metal ions as neighbors, whereas only metal ions are located at this distance from the octahedral site.

The presence of CuO in some samples further complicates this analysis since the binary oxide also has a peak at 3.0 Å. Nevertheless, a reasonable concentration of octahedrally coordinated Cu^{2+} ions can be inferred for both catalyst Nos. 16 and 20. When catalyst No. 16 was heated to 900°C, yielding catalyst No. 18, the amount of octahedral ions appears to decrease from the disappearance of the 2.8 Å peak. Cupric ions in catalyst No. 2 appear to be octahedrally coordinated because of the absence of the 3 Å peak, whereas the low intensity of the 2.8 Å peak may indicate that few octahedral sites are next near neighbors to each other or else their vibrational motion is poorly correlated, analogous to findings in comparisons of amorphous and crystalline semiconductors (*29*).

These qualitative arguments can now be compared to quantitative values for the first shell coordination numbers and distances shown in Table 5. Assuming only octahedral and tetrahedral sites for cupric ions, the relative percentages of each environment can be calculated from the coordination numbers. The implications of these results is discussed in more detail below in conjunction with the information from the other techniques.

DISCUSSION

Copper catalysts have been investigated by a gamut of physical techniques. First we shall summarize this previous work and then discuss our results and their relation to it. As early as 1948, Selwood and Dallas (*30*) noted a decrease in the magnetic susceptibility per unit metal of samples with loadings greater than 10 to 11 wt% copper on a 200 m^2/g γ-Al_2O_3 support, and furthermore, that supported "copper oxide" has a higher magnetic susceptibility per metal atom than the bulk material. The metal loading for the transition also corresponded to the appearance of bulk CuO in the X-ray diffraction pattern. Matsunaga (*22*) extended the picture by comparing

FIG. 4. Fourier transformed Cu K-absorption edge EXAFS (data over range k = 4.1 to 11 $Å^{-1}$): (a) CuO; (b) $CuAl_2O_4$; (c) catalyst No. 2 (6.1% Cu/KA201(c)/500°); (d) catalyst No. 16 (8.9% Cu/AL0104/500°); (e) catalyst No. 20 (16% Cu/AL0104/500°); (f) catalyst No. 18 (8.9% Cu/AL0104/900°).

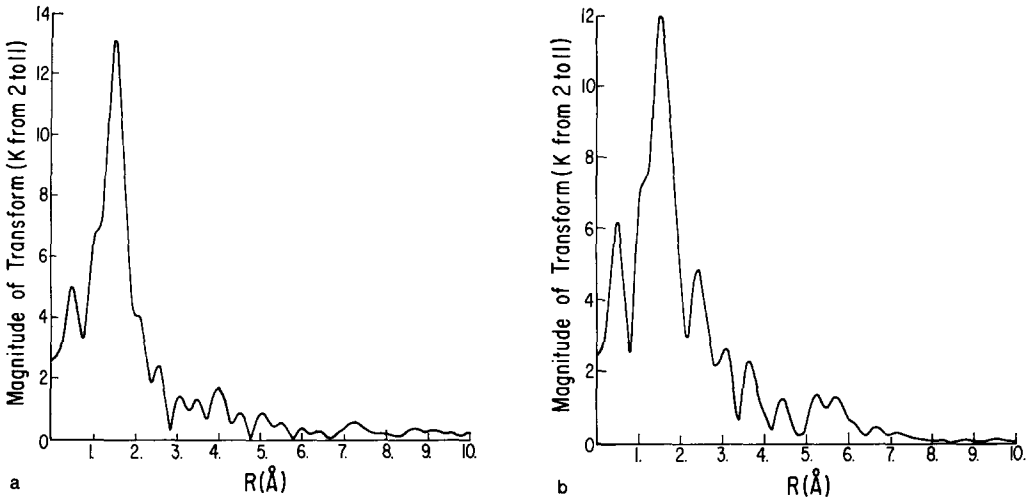

FIG. 5. Fourier transformed Cu K-absorption edge EXAFS (data over range k = 2 to 11 Å^{-1}): (a) catalyst No. 2 (6.1% Cu/KA201(c)/500°); (b) catalyst No. 16 (8.9% Cu/AL0104/500°).

ESR with the magnetic susceptibility results. He concluded that in addition to bulk CuO there are two kinds of dispersed states. One kind contributes to both magnetic susceptibility and resonance absorption, whereas the other does not give a detectable ESR signal. It was proposed that the latter is broadened into the background by interaction with neighboring cupric ions. Other ESR work by Berger and Roth (*2*) analyzed the signal in terms of a tetragonally distorted octahedrally coordinated cupric ion broadened by magnetic interactions with surrounding paramagnetic ions.

As mentioned above, X-ray diffraction shows no copper-containing phase at low loading prepared by low temperature calcination. At higher metal levels, the characteristic pattern of CuO is seen, whereas at higher calcination temperatures (>700°C) bulk $CuAl_2O_4$ is detected (*1, 3, 5*) Wolberg *et al.* also used ESCA (*4*) and K-absorption edge shifts (*3*) to distinguish between CuO and an aluminate phase on the supports. They found that the copper

TABLE 5

Coordination Parameter for $CuAl_2O_4$ and Cu/γ-Al_2O_3 Catalysts

Material	r_1 Å	N_1	Percentage	
			$(O_h:T_d)^a$	$(O_h:T_d)^b$
Catalyst No 18 (8.8% Cu/AL0104/900°)	1.91 ± 0.05	4.4 ± 0.5	20:80	40:60
$CuAl_2O_4$, 32.7% Cu 962°C calcination	1.94	4.8	40:60	
Catalyst No. 2 (6.1% Cu/KA201(c)/500°)	1.98	5.2	50:40	100:0

[a] Let X = fraction of Cu in tetrahedral sites, then $X(4) + (1 - X)6 = N_1$; $X = (6 - N_1)/2$.

[b] Values calculated if the octahedral site has only five neighbors. ($X = 5 - N_1$).

on a high surface area alumina was typified by an aluminate, whereas at a high level of metal on a lower surface area support, CuO was predominant. The aluminate phase was detected even on material calcined as low as 300°C. Since bulk $CuAl_2O_4$ has both octahedral and tetrahedral sites occupied by cupric ions (*15*), an additional question arose when Summers and Klimisch (*5*) reported their results of an optical study as showing only octahedrally coordinated cupric ions on the alumina supports. Roth (*6*) proposed that the discrepancy could be resolved if it was assumed that ESCA and *K*-edge techniques can distinguish between Cu^{2+} in CuO and $CuAl_2O_4$, but not between the different coordination environments within the spinel. This explanation was no longer sufficient when Lytle and co-workers (*31*) concluded from their EXAFS study that both 4- and 6-coordinate cupric ions were present in $CuCr/Al_2O_3$ catalysts. More recent reports of optical spectra of Cu/Al_2O_3 catalysts identify both octahedral and tetrahedral Cu^{2+} (*9, 11*); elsewhere we have proposed an explanation (*10*) for the oversight by Summers and Klimisch.

Consideration of this prior work with our data in Fig. 1B clearly indicates that there are two gross regimes that must be considered (a) the initial interaction with the support, and (b) after agglomeration of bulk CuO. The linearity of the relationship in Fig. 1B can be interpreted to show that beyond a critical quantity, any additional copper loading is in the form of bulk crystalline oxide. At the time that Fig. 1B was prepared, analytical data were not available for catalyst No. 19. Using the plot, a copper content of 9.1 wt% was predicted, in excellent agreement with the value of 8.9 wt% Cu ultimately determined by conventional analytical methods.

From these data we can extract a support capacity of 3.5 wt% Cu/100 m^2/g for AL0104 γ-alumina. From our observation of the appearance of CuO in catalyst No. 2, prepared using KA201(c), we obtain a loading capacity of 3.7 wt% Cu/100 m^2/g. Jacobson and Selwood (*32*) report similar results on a homemade alumina, 7.5 wt% Cu on a 250 m^2/g support (3 wt% Cu/100^2/g). The work of Summers and Klimisch (*5*) yields a value of 5.5 wt% Cu/100 m^2/g on KA302 support, whereas 5 to 5.5 wt% Cu/100 m^2/g is deduced from data from Selwood and Dallas (*30*). A change in a number of properties also appears to be correlated with this support capacity: the magnetic susceptibility (*30, 32*), CO adsorption (*33*) and catalytic activity (*16, 34*). The total number of adsorption sites appears to be generally related, but not exactly proportional, to the surface area, approximately 4 wt% Cu/100 m^2/g for the different γ-aluminas. These support sites appear to be saturated before development of a separate crystalline copper phase (*vide infra*). This behavior is not general; it is in marked contrast to Co/Al_2O_3 system (*35*), where the bulk spinel Co_3O_4 appears to grow, perhaps epitaxially, on the support concurrently with the dispersed phase.

If both crystalline and dispersed phases are present at the higher loadings, then we must explain the success of the previously reported correlations with ESCA and *K*-edge shifts which showed the exclusive presence of one or the other phase.

The observed Cu $2p_{\frac{3}{2}}$ photoemission peaks have a full width at half maximum between 2.5 and 4.5 eV, whereas the binding energy difference between the unsupported binary oxide and bulk copper aluminate is only 1 eV; thus, the peaks are not easily resolvable. Furthermore, ignoring any effects of charge dispersion or other pitfalls of quantification, the relative peak heights for equal quantities of the two phases would naively be expected to be inversely proportional to their relative peak widths; i.e., the $CuAl_2O_4$ peak should be about 1.5 times as prominent as the CuO peak. Therefore, the use of the

maximum of the observed peak to determine the binding energy would preferentially favor identification of aluminate as the predominant phase in a catalyst. The extra peak width, at most 0.5 eV, would not be conspicuous for these insulating materials. Since the previous workers used samples in the extreme composition limits with either no CuO or a threefold predominance of the oxide, the binding energy correlation with phase identity was clearcut. Those of our samples with CuO, but not nearly as dominant an excess, catalyst Nos. 16 and 19, were a more severe test. In these instances, the features of the individual spectra determined whether the assignment was in terms of a single phase or a mixture.

The *K*-edge correlation has a similar limitation. The edge for CuO is at lower energy than that of $CuAl_2O_4$. The appearance of CuO follows the presence of the "aluminate" and therefore CuO is easily detected by the earlier onset of an increased X-ray absorption. In the present work, the determination of the edge position by its inflection point is more reflective of the edge structure and the presence of two phases. Finally, in the extreme case of catalyst No. 20, with the overwhelming predominance of CuO, the assignment of CuO is clear regardless of the method of locating the peak in the X-ray absorption and ESCA experiments. Thus, Roth's proposition (*6*) is correct; i.e., these deep hole probes can distinguish between the two phases but not between the different geometric coordinations within the spinel. Although we shall not try to explain the binding energy differences, we can question the role of relaxation about the core hole since the Auger parameters (*36*), which should be a more sensitive probe of this effect, are the same for both compounds.

As we have shown for ESCA and *K*-edge positions, the properties of catalysts in this composition range are a superposition of those of copper oxide and the dispersed cupric ions. The magnetic susceptibility and ESR results, presented on a per atom basis, asymptotically approach the bulk value. Nevertheless, the mere detection of the characteristic ESR signal at very high copper loadings demonstrates the existence of a dispersed phase. Bulk CuO has a very different broad signal.

Let us now consider the mode of interaction of the cupric ions with the support from the dilute limit to the support capacity. Optical spectra invariably show cupric ions in both tetrahedral and octahedral coordination. Although tetragonal distortion of the octahedral environment could also explain a peak in the near infrared region, Kassman (*9*) has quantitatively analyzed the spectra and found the low energy band to be bimodal with components from a tetrahedrally coordinated cupric ion and from cupric ions in a C_{4v} environment. This two-peak structure is also apparent in our spectra of a catalyst prepared in a wet atmosphere (*10*). The presence of both coordination environments is also consistent with the EXAFS results.

The ESR results have been interpreted solely in terms of the distorted octahedral site symmetry; however, the absence of a signal for a tetrahedral species should not be too of great concern. Relaxation times for Cu^{2+} in tetrahedral environments have often been short enough that signals were observable only at very low temperatures (*37*). Furthermore, if some tetragonal distortion were present, the resonance peaks would appear at similar g values as for the distorted octahedron and only the hyperfine splittings would differ (*19*, *37*). This would not be detectable when overwhelmed by the presence of the octahedral species.

Comparison of the semiquantitative optical results and the EXAFS coordination numbers (Table 5) is also revealing. Even allowing for the large uncertainty in the coordination numbers and hence in the calculated cation distribution, it appears

reasonable to invoke a "5-coordinate octahedral" site. This does not preclude the presence of a loosely bound sixth ligand. As frequently mentioned, this is also consistent with optical (*9*) and ESR (*2*) models. The interesting feature is the fact that this distortion may persist in the "dispersed surface copper aluminate" formed by sintering the alumina-supported copper catalysts. Although X-ray diffraction and optical spectra show typical bulk copper aluminate, the EXAFS coordination numbers must be stretched to the limit of their experimental uncertainty. Upon reflection, this is not as startling as it initially appears. Bulk $CuAl_2O_4$ has a surface enrichment of cupric ions compared to bulk stoichiometry (*8, 38*); an observation of more general nature for Cu^{2+} in octahedral coordination in metal oxides (*8, 38, 39*). Earlier ESR work had shown the accessibility of the cupric ions to the gaseous environment in samples sintered at 900°C for 5 days (*41*), hence, their presence in an exposed site on the surface. The resonance itself is also indicative of the continued dispersion of the phase since bulk $CuAl_2O_4$ has no detectable signal; its absence has been attributed to antiferromagnetic interactions between the transition metal cations. Comparison of catalyst No. 4 with No. 6 (Figure 2b and c) and catalyst No. 2 with No. 8 (similar but not displayed) shows that heating the catalysts to 600°C results in an increase in tetrahedrally coordinated Cu^{2+}. The noticeable effect on the tetrahedral band while the octahedral band appears unchanged is a consequence of the high ratio of 6-coordinate to 4-coordinate ions and their relative absorption coefficients; therefore, the observed change in spectra undoubtedly reflects only a small redistribution of the total cations present. Nevertheless, these observations coupled with studies reported elsewhere (*5, 7, 15*) appear to indicate that the cation redistribution can proceed to the ultimate formation of the aluminate with the proper combination of time with temperatures over 600°C.

The "aluminate phase" detected by ESCA and *K*-edge methods is NOT necessarily thin, X-ray transparent domains analogous to the bulk material. Not only can the cation distribution be different, but bulk studies have shown that $CuAl_2O_4$ is unstable relative to Al_2O_3 and CuO at temperatures <612°C (*41*). In contrast, the surface spinel has been prepared at 300°C (*3*). The bulk aluminate is a magnetically concentrated material with no detectable ESR signal. As a natural consequence of their dispersion, the supported cupric ions do show an asymmetric resonance typical of Cu^{2+} in an axial environment, but the signal is broadened by dipolar interactions with neighboring paramagnetic ions (*42*). Furthermore, only a small fraction of the cupric ions contribute to the ESR signal (*2, 40*). The similar lineshape and the absence of a plateau in the intensity per atom would indicate that cooperative effects and clustering exist even at low loadings, contrary to a model of random site distribution (*43*). This does not require the existence of either CuO or $CuAl_2O_4$ since the literature is replete with examples of magnetic interactions between cupric ions in a wide variety of materials (*44*).

Roth (*45*) has shown that the adsorptive capacity of aluminas from excess copper nitrate solutions depends much more on their chemical modification than surface area. Although the adsorptive capacity by this exchange method was only ~1.5 wt% Cu/100 m^2/g, preparation by minimum solution methods involves sufficiently different conditions that a higher saturation limit for the supports can be rationalized by either a surface complex (*46*) or ion exchange (*47*) model. The limitations of deposition at higher loading is also visually apparent during preparation. In the course of drying, the liquid phase moves out of the pore structure. Apparently, during the

final stages the cupric ions are very weakly bound by the support and a chromatographing effect occurs. A black coating, CuO, is seen on the upper surface of the particles at the top of the catalyst bed. When the sample is ground, the level of CuO is below detection by X-ray diffraction (~0.5 wt%). This appearance as a shell structure is distinct from the pervasion of the formed support by the oxide when the support capacity is exceeded. There are more than sufficient hydroxyl groups on γ-Al_2O_3 to accommodate the support capacity (~4 wt% Cu/100 m^2/g) discussed in this work (*48*). After drying and calcination, however, the cupric ions must be tightly bound to the support since these catalysts with adsorbed bases show only a small perturbation of the optical spectra of freshly degassed samples (Fig. 3). By contrast, Cu^{2+}-exchanged Y zeolites change color from light green to blue or purple after similar treatment (*49*); this effect has been quantitatively measured by their photoacoustic spectra (*50*).

Finally, there is evidence that CuO does not exist in X-ray transparent domains as the support capacity is approached. The EXAFS radial distribution function for catalyst No. 2, just at the capacity loading, does not show the distinct structure of CuO in the 4 to 6 Å region as might be expected if a reasonable concentration of CuO domains between 20 and 50 Å were present. As the CuO clusters increased in number and size, optical absorption in the region about 500 nm should increase. The minimum in this region for the dispersed cupric ions persists until bulk CuO is also detected by X-ray diffraction. If a random site model were correct and if essentially all the cupric ions were to become part of bulk CuO at very high loadings, then the extrapolation of the line in Fig. 1B from these high loadings should pass through the origin. Our method of determining the loading capacity actually should avoid any problems associated with limitations on the X-ray diffraction technique from domain size. Any anomalous behavior of this type should manifest itself just above the threshold level for agglomeration; none was noted.

SUMMARY

A variety of physical techniques was used to study the interaction of cupric ions with transition aluminas. A unified picture of the phases present and the cation site locations has been formulated using the diverse results. At low concentrations copper enters the defect spinel of the γ-alumina support to yield a well dispersed phase which is not detected by X-ray diffraction. The immediate site location is predominantly a tetragonally distorted octahedron although ~10% of the ions are in tetrahedral environments. At temperatures $\gtrsim$600°C, there is a kinetically limiting transformation tending toward the bulk spinel cation distribution. The support capacity for a number of different γ-aluminas appears similar and generally related to their surface areas, ~4 wt% Cu/100 m^2/g. In this dispersed phase, even up to the highest copper loading, the cations are NOT in microcrystals of CuO. The environment more closely resembles the aluminate but the transition metal cation locations and interactions with each other can differ widely from the bulk material. After the adsorption sites of the support are saturated, a discrete crystalline phase of clustered copper oxide forms on the surface as detected by its X-ray diffraction pattern.

ACKNOWLEDGMENTS

Dr. P. A. Berger kindly provided the E.S.R. data and numerous informative discussions. Drs. J. Ogilvie and H. Yuen, and Messrs. F. May and J. Brumbaugh performed the ESCA, surface area, X-ray diffraction and analytical measurements, respectively. Discussions with Drs. J. F. Roth, N. A. Fishel, and J. W. Gambell are greatly appreciated. Furthermore, Dr. Roth is warmly

acknowledged for the initial suggestion and stimulus for pursuing this problem. The EXAFS data for metallic copper, CuO, Cu_2O, and $CuCl_2 \cdot 2H_2O$ were obtained on an identical instrument to ours by Dr. G. Via, Exxon Research and Engineering Co., Linden, N.J. He has generously given us permission to use them for the purpose of this investigation.

REFERENCES

1. Pierron, E. D., Rashkin, J. A., and Roth, J. F., *J. Catal.* **9**, 38 (1967).
2. Berger, P. A., and Roth, J. F., *J. Phys. Chem.* **71**, 4307 (1967).
3. Wolberg, A., and Roth, J. F., *J. Catal.* **15**, 250 (1969).
4. Wolberg, A., Ogilvie, J. L., and Roth, J. F., *J. Catal.* **19**, 86 (1970).
5. Summers, J. C., and Klimisch, R. L., *Proc. Int. Congr. Catal., 5th, 1972* **1**, 293 (1973).
6. Roth, J. F., *Proc. Int. Congr. Catal., 5th, 1972* **1**, 302 (1973).
7. Roth, J. F., *Ind. Eng. Chem., Prod. Res. Develop.* **10**, 381 (1971).
8. Shelef, M., Wheeler, M. A. Z., and Yao, H. C., *Surface Sci.* **47**, 697 (1975).
9. Kassman, A., Paper INOR 86, presented: 167th Natl. Meeting of the Amer. Chem. Soc., Spring, 1974, Los Angeles; and private communication to R. M. Friedman (1976).
10. Friedman, R. M., and Freeman, J. J., *J. Chem. Soc., Trans. Faraday I* 758 (1978).
11. LoJacono, M., and Schiavillo, M., "Preparation of Catalysts" (B. Delmon, P. A. Jacobs, and G. Poncelet, Eds.), p. 473. Elsevier, Amsterdam, 1976.
12. Thomas, C. L., "Catalytic Processes and Proven Catalysts," p. 198. Academic Press, New York, 1970.
13. Although dealing specifically with silica supports, see Roman A., and Delmon, B., *J. Catal.* **30**, 333 (1973), and references therein.
14. Roth, J. F., and Gambell, J. W., Soc. Automotive Engr., Intl. Automotive Engr. Congr., Detroit, Michigan, 730277 (1973).
15. Friedman, R. M., and Dahm, D. J., in preparation.
16. Friedman, R. M., and Bauer, D. J., unpublished data.
17. Berger, P. A., Moog, R., and Friedman, R. M., unpublished data.
18. Friedman, R. M., Lytle, F. W., and Freeman, J. J., unpublished data.
19. Friedman, R. M., Lytle, F. W., Freeman, J. J., and Berger, P. A., unpublished data.
20. (a) Lytle F. W., Sayers, D. E., and Stern, E. A., *Phys. Rev. B* **11**, 4825 (1975); (b) Stern, E. A., Sayers, D. E., and Lytle, F. W., *Phys. Rev. B* **11**, 4836 (1975); (c) Lytle F. W., and Friedman, R. M., in preparation for publication.
21. Tandon, S. P., and Gupta, J. P., *Spectrosc. Lett.* **3**, 297 (1970), and references therein.
22. Matsunaga, Y., *Bull. Chem. Soc. Japan* **34**, 1291 (1961).
23. Verma, L. P., and Agarwal, B. K., *J. Phys. C* **1**, 1658 (1968).
24. (a) Kortum, G., "Reflectance Spectroscopy." Springer-Verlag, New York, 1969; (b) Klier, K., *Catal. Rev.* **1**, 207 (1967); (c) Surles, T., Erickson, J. O., and Priesner, D., *Amer. Lab.* 55 (March 1975).
25. Papalardo, R., *J. Mol. Spectrosc.* **6**, 554 (1961).
26. Hayes, T. M., and Sen, P. N., *Phys. Rev. Lett.* **34**, 956 (1975).
27. Bingham, C., Godfrey, M., and Tukey, J., *IEEE Trans. Audio Electroacoustics* **AU-15**, 56 (1967).
28. Stern, E. A., *Phys. Rev. B* **10**, 3027 (1974).
29. Hunter, S. H., Ph.D. thesis, Stanford Univ., 1977; (a) Bassi, I. W., Lytle, F. W., and Parravano, G., *J. Catal.* **42**, 139 (1976).
30. Selwood, P. W., and Dallas, N. S., *J. Amer. Chem. Soc.* **70**, 2145 (1948).
31. Lytle, F. W., Sayers, D. E., and Moore, E. B., Jr., *Appl. Phys. Lett.* **24**, 45 (1974).
32. Jacobson, P. E., and Selwood, P. W., *J. Amer. Chem. Soc.* **76**, 2641 (1954).
33. Kostrov, V. V., Kirillov, I. P., Akulickev, Y. F., and Smirnov, V. A., "Preparation of Catalysts" (B. Delmon, P. A. Jacobs, and G. Poncelet, Eds.), p. 293. Elsevier, Amsterdam, 1976.
34. Mooi, J., and Selwood, P. W., *J. Amer. Chem. Soc.* **74**, 2461 (1952). {A capacity value required assuming a support surface area; analogy to other work from that laboratory [Refs. (30, 32)] would suggest 200 to 250 m^2/g to be reasonable}.
35. Declerck-Grimée, R. I., Canesson, P., Friedman, R. M., and Fripiat, J. J., *J. Phys. Chem.* **82**, 885 and 889 (1978).
36. Wagner, C. D., *Anal. Chem.* **47**, 1201 (1975); *Faraday Discuss.* **60**, 291 (1975).
37. deWit, M., and Reinberg, A. R., *Phys. Rev.* **163**, 261 (1967).
38. Barber, M., Sharpe, P. K., and Vickerman, J. C., *J. Catal.* **41**, 240 (1976).
39. Goldobin, A., and Savchenko, V., *Kinet. Katal.* **15**, 1363 (1964).
40. Lumbeck, H., and Voitländer, J., *J. Catal.* **13**, 117 (1969).
41. Jacob, K. T., and Alcock, C. B., *J. Amer. Ceramic Soc.* **58**, 192 (1975).
42. Fujiwara, S., Katsumata, S., and Seki, T., *J. Phys. Chem.* **71**, 115 (1967).

43. Poole, C. P., Jr., *J. Phys. Chem.* **67**, 1297 (1963).

44. Kato, M., Jonassen, H. B., and Fanning, J. C., *Chem. Rev.* **64**, 99 (1964).

45. Roth, J. F., private communication, 1975.

46. Schindler, P. W., Fürst, B., Dick, R., and Wolf, P. U., *J. Colloid Interface Sci.* **55**, 469 (1976).

47. (a) Dugger, D. L., Stanton, J. H., Irby, B. N., Connell, B. L., Cummings, W. W., and Maatman, R. W., *J. Phys. Chem.* **68**, 757 (1964); (b) Greenberg, S. A., *J. Phys. Chem.* **60**, 325 (1956).

48. Santacesaria, E., Gelosa, D., and Carr, S., *Ind. Eng. Chem., Prod. Res. Develop.* **16**, 45 (1977).

49. (a) Williamson, W. B., and Lunsford, J. H., *J. Phys. Chem.* **80**, 2664 (1975). (b) Egerton, T. A., Hardin, A., and Sheppard, N., *Canad. J. Chem.* **54**, 586 (1976).

50. Freeman, J. J., and Friedman, R. M., unpublished data.